

Pulse position modulated (PPM) ground receiver design for optical communications from deep space

A. Biswas, V. Vilnrotter, W. Farr, D. Fort and E. Sigman

*Jet Propulsion Laboratory, California Institute of Technology,
4800 Oak Grove Drive, Pasadena, CA 91109-8099*

ABSTRACT

Pulse position modulation (PPM) provides a means of using high peak power lasers for transmitting communications signals from planetary spacecraft to earth-based receiving stations. Large aperture (~10 m diameter) telescopes will be used to collect and focus the laser communications signal originating from a deep space transmitter on to a PPM receiver. Large area (1- 3 mm diameter) sensitive detectors preceded by appropriate narrow (0.1- 0.2 nm) optical band-pass filters and followed by low-noise, high-gain, amplifiers will serve as the PPM receiver front end. A digital assembly will form the backbone of the receiver. The PPM receiver must achieve and maintain slot synchronization based on sub slot sums provided by a field programmable-gated array (FPGA). Spacecraft dynamics and timing issues between the ground-based receiver and the transmitter on board the spacecraft must be taken into account. In the present report, requirements and design of a prototype PPM receiver being designed for development over the next year will be elaborated. The development is driven by the need to demonstrate and validate PPM reception using a variety of detectors under simulated conditions representative of those to be encountered in a deep space optical communications link.

Keywords: pulse-position modulation, avalanche photodiodes, photomultiplier tube, slot synchronization

1. INTRODUCTION

Ground reception technology for deep space optical communications is being developed at JPL in order to service future NASA missions. Increased data rates accompanied by a reduction in payload mass, volume and power, motivate development of technology required for optically communicating with interplanetary spacecraft. The baseline concept relies on using earth-based receiving stations to detect pulse position modulated (PPM) laser signals transmitted from a spacecraft located at planetary distances. Adequate signal photons for achieving uncoded bit error rates (BER) of approximately 10^{-2} are required in order to establish an optical link.¹ Coding techniques will be used to provide improved BER's of 10^{-5} . Link analysis has shown² that high peak power laser transmitters on board planetary spacecraft, equipped with the ability to point narrow divergence laser beams back to earth, can return the required signal photons to earth. Large area (~10 m diameter) collecting apertures will be used to focus the optical signal on to large area³ (~2 - 3 mm diameter) sensitive detectors. Appropriate narrow (0.1-0.2 nm) optical band-pass filters, preceding the detectors will be used to reject background signal from incidence upon the detectors. Detectors with associated analog and digital electronics constitute the PPM receiver that is the subject of the current report.

The PPM receiver shall consist of three major functional units, namely, (1) a front-end optoelectronic detector (2) an analog signal chain (ASC) that conditions the output of the detector and (3) digital signal processing assembly (DSP) for further processing to extract the information. A block diagram depicting these units is shown in Figure 1. Details of the optoelectronic detector are discussed elsewhere⁴. This report will emphasize the requirements and design for the ASC and DA. In addition analysis and discussions of how the PPM receiver will enable anticipated operations scenarios will be presented. The prototype PPM receiver design shall be based upon available detectors and electronics, and will also baseline the use of a q-switched laser transmitter.

The prototype PPM receiver is intended for rigorous laboratory and field-testing. Some of the intended testing is categorized below and influences design choices.

- (1) End-to-end laboratory testing under simulated laboratory conditions that will enable measurement of BER versus photons per bit using a variety of detectors.

- (2) Field demonstrations where laser beams are transmitted across a near horizontal atmospheric path prior to impinging on a 0.6-1m diameter telescope that guides the photons to a receiver located at the focal plane. Alternately the laser could be transmitted over an atmospheric path through the receiving telescope and retro-reflected prior to incidence on the receiver.
- (3) Retro-reflected links to satellites where short duration (~15 ms) bursts of pulses are transmitted and retro-reflected in order to test receiver functions while tracking satellites.

By first assembling the prototype PPM receiver and then performing some of the tests described above, risks involved in implementing optical communications as a means of retrieving data from spacecraft at planetary distances will be minimized. This will also provide a theoretically sound and experimentally validated basis for more advanced designs of future receivers required for providing a robust high data rate service for NASA's future missions. In section 2 an overview of the optical PPM receiver design is described, followed by a discussion of operational considerations in section 3. Section 4 will present discussions related to synchronization whereas section 5 and 6 will describe the ASC and DSPA followed by conclusions in section 6.

2. PPM RECEIVER DESIGN OVERVIEW

A block diagram of the optical receiver is shown in Figure 1, where the major functional blocks are identified and their interconnection specified. The front end consists of a detector assembly, which can be either a conventional avalanche photodiode (APD) detector or a photomultiplier tube (PMT), selectable by the user.

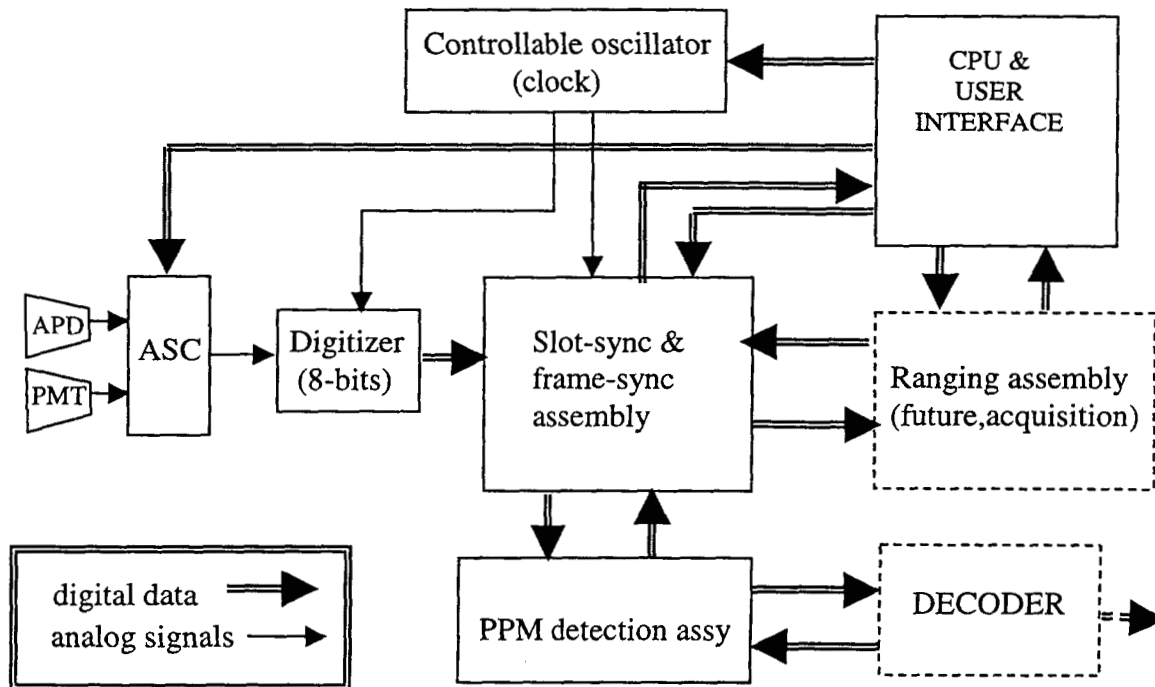


Figure 1. Optical PPM receiver functional block diagram showing analog and digital inter-connections.

In addition to enabling the evaluation of a variety of detectors, the ability to switch the front-end supports operations: for example, under daytime background levels APD's may be desired while the much lower nighttime background levels can take advantage of more sensitive PMT's. The output of each detector is connected to conditioning circuits via a user selectable switch, for amplifying the detected signal and establishing a suitably high signal-to-noise ratio (SNR): for the APD detector this operation typically requires a matched transimpedance amplifier, whereas for the PMT a wideband follow-on amplifier will be required.

The analog signals are conditioned and then digitized to eight bits at a rate determined by the system clock. Because of ease of availability, complexity, cost-effectiveness and prior experience the PPM receiver design will be based upon a nominal 200 MHz clock. The digitized signal will be input to the *slot synchronization*, and *PPM detection* assemblies. The

receiver will have a dedicated central processing unit (CPU) for user interface and data storage. Provision will be made for later implementation of a ranging and decoding assembly shown as dashed boxes in Figure 1.

Figure 2a shows a schematic representation of the PPM timing arrangement. T_w represents the word or frame time and is comprised of a symbol time MT_s (M is the alphabet size and T_s is the slot width) and a dead time T_d that for q-switched lasers is the minimum time required for the population inversion of the laser to build up prior to emitting a pulse. Note that for q-switched lasers the dead time is the inverse of the pulse repetition rate of the laser as opposed to diode lasers where T_w is the reciprocal of the laser repetition rate.

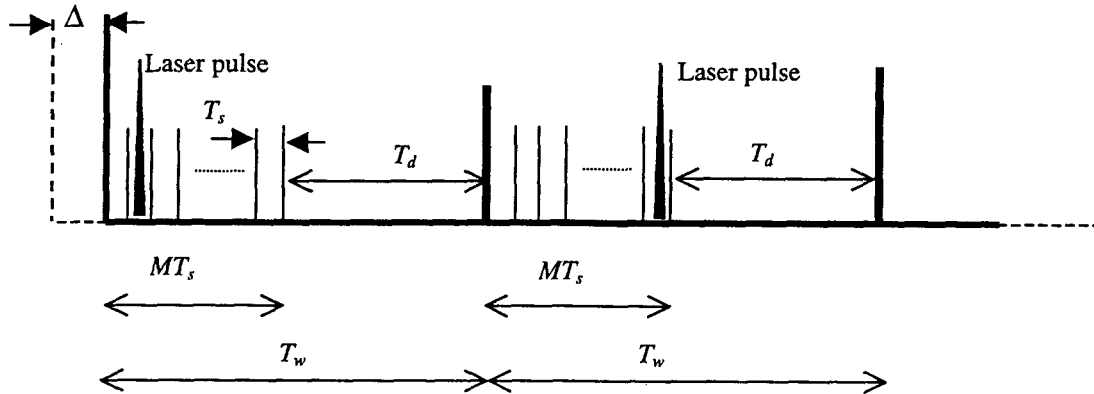


Figure 2 Schematic representation of the PPM timing scheme, T_s represents the slot width, T_d is dead time (the minimum time required for a q-switch laser to build up energy prior to emitting a pulse), M is the alphabet size and T_w is a PPM word time.

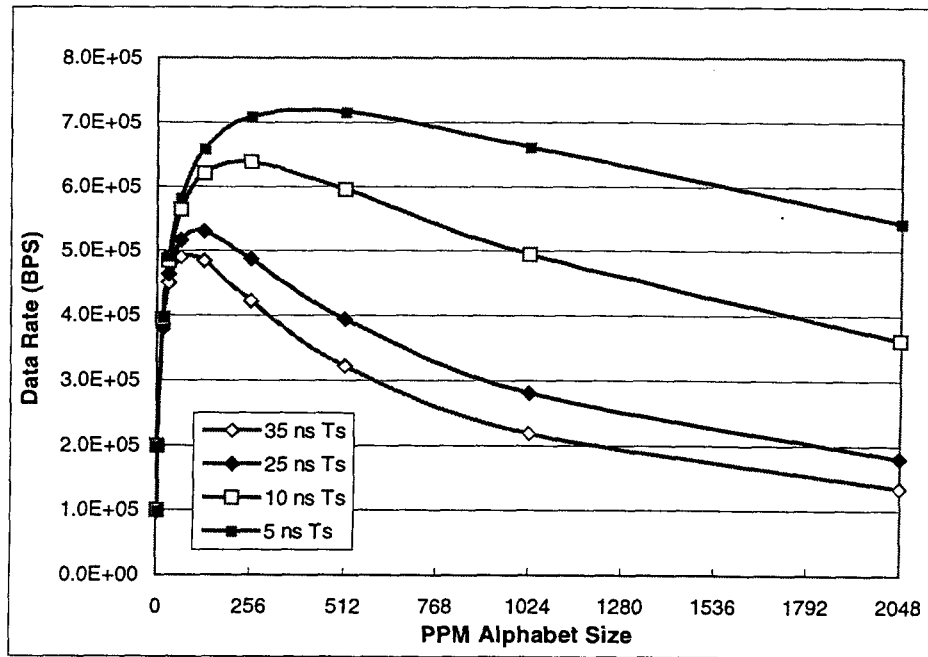


Figure 3 The dependence of data rate upon PPM alphabet size for a q-switched laser capable of 100 K pulses per second ($T_d = 10 \mu\text{sec}$)

The slot location of the PPM laser translates into a bit value. For example, with $M = 256$ the laser pulse occurring in the first slot would be translated to a zero, whereas, in the last slot it would represent 255. Thus a single laser pulse can be used to carry 8-bits of data. As an example, a q-switched laser transmitter capable of emitting 100 K pulses per second Figure 3 shows a family of curves corresponding to different slot widths (T_s) that show the variation of data rate with alphabet size, for

a given dead-time, chosen to be 10 μ sec here. This relationship shows that the maximum data rates are obtained for values around 128, namely, $M=64$, 128 and 256. The choice of slot width influences the peak of the curves with a shift toward lower M values for larger values of T_s . The slot width should be adequate to accommodate the laser pulse width plus some allowance for pulse jitter inevitably associated with q-switching. This calls for T_s to be larger than T_p perhaps by 20%. T_p is a convolution of the emitted laser pulse width and the detector response. Available detectors that display desirable sensitivity characteristics for detection of faint signals have limited impulse response bandwidth that restricts T_p to be no less than 8-10 ns even though q-switch lasers are capable of emitting narrower pulses (2.5 ns, for example). On the other hand the greater T_s the more background light photons are collected within the field-of-view of the detector. Thus the ability to reduce T_s by developing detectors with greater bandwidth that provide improved values of T_p would benefit the optical link. Of course as T_s is made smaller the digitizer speed also needs to be increased in order to provide adequate sampling. Given the current detectors and lasers that will be available for testing, the 200 MHz clock (5 ns) sampling will be adequate for the PPM receiver we are planning to develop.

A 5 ns sampling time supports a minimum 10 ns slot width T_s since at least two sub-slots are required in order to establish slot synchronization, while there is no upper limit on the number of sub-slots per slot provided they are even. We are assuming that the transmitter clock also runs at 200 MHz, generating 5 ns clock edges for controlling the firing of the transmitter laser. As mentioned above, PPM modulation consists of mapping each sequence of L data-bits into one of $M = 2^L$ slot-locations according to a predetermined look-up table, and firing the laser so as to place the optical pulse in the correct slot relative to the previous pulse. After firing there is a recovery time during which the laser cannot be fired, giving rise to a "dead-time" following each pulse: this interval is 10 μ sec for a laser capable of emitting 100K pulses per second. With no loss in generality, we assume that there is a dead-time of exactly N slots following the M signal slots, for a total of $M+N$ "frame" slots.

The transmitted optical pulse propagates to the receiver over free space at a rate of approximately three nanoseconds (nsec) per meter. In the laboratory the distance between the transmitter and the receiver is typically on the order of meters, whereas in field testing over horizontal paths or with near earth satellites it can be tens to hundreds or thousands of kilometers. The finite propagation time gives rise to a delay that is generally not known with great accuracy, and may in addition be varying with time as the range to satellite varies. This relative delay represented by the symbol Δ in Figure 2, and can be thought of as a shift between the origin of the time axes at the two locations: the main purpose of slot synchronization is to establish a one-to-one correspondence between the receiver clock and the transmitter clock following pulse propagation through the physical channel, so that measurements can be carried out at the receiver over time intervals that contain the entire laser pulse after it arrives. In addition, the slot boundary corresponding to the start of the PPM symbol has to be determined before decoding, or PPM symbol detection, can take place.

3. OPERATIONAL CONSIDERATIONS

When attempting to track a fast-moving object such as a spacecraft, particularly one with rapidly changing velocity, the impact of spacecraft dynamics on the PPM pulse-train must be taken into account. Consider the communications link depicted in Fig. 4, showing a spacecraft in relative motion with respect to the receiver. The velocity vector of the spacecraft can be decomposed into radial and tangential components with respect to the receiver, which is assumed to be a stationary receiver on the ground. The tangential component gives rise to angular motion which must be tracked by the receiving telescope, while the radial component gives rise to temporal dynamics. We assume here that the tangential component is tracked by the telescope, and concentrate only on temporal effects.

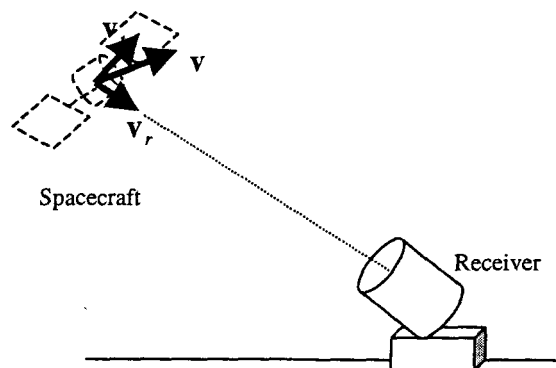


Figure 4 Typical configuration of spacecraft with respect to an earth based receiver.

Suppose the radial velocity v_r is towards the receiver, as in Fig. 4, with magnitude v_r (much less than the velocity of light, c , so that relativistic effects can be ignored) and the transmitter aboard the spacecraft is sending a train of pulses as depicted in Fig. 2. For this analysis it is easiest to assume that the pulse is always in the first of $M + N$ slots, which includes both information and "dead-time" slots. The clocks at the ground receiver and aboard the spacecraft are assumed to be synchronized. Although we are ignoring relativistic effects, we can state this condition precisely by assuming that the two clocks were synchronized at some earlier time when the relative radial velocity component was zero, and that the clocks are stable enough to keep any relative drift between them negligibly small. To simplify the analysis, we further assume that the transmitted pulses are in the first slot of each frame. There are three cases to consider: zero radial velocity, positive radial velocity (taken to be towards the receiver), and negative radial velocity (away from the receiver). In the first case each subsequent pulse arrives at a fixed delay $\Delta = R/c$ later where R is the range to the spacecraft and c is the velocity of light. Provided the time of arrival is known (through the use of predicts, for instance) the pulse arrival time can be made to coincide with the center of the first receiver slot by adjusting the clock. For a positive or negative radial velocity, respectively, the N^{th}

pulse arrives $(N-1)T_w \left(1 \mp \frac{v_r}{c}\right)$ after the first pulse, where $T_w = (M+N)T_s$. Therefore the frame time is

compressed/expanded depending on the sign of v_r . In order to stay synchronized with incoming pulses the receiver must continuously reduce/increase frame duration. An interesting extension of this analysis is for the case where the pulses are retro-reflected from a satellite. Because of the range to the satellite R a large $(1/R^4)$ loss associated with retro-reflected links they are not practical for interplanetary distances, however, they may prove very useful where a PPM laser sequence generated on the ground can be retro-reflected from nearby earth orbiting satellites in order to test the receiver's ability to acquire and establish synchronization. In this case the frame time compression factor assumes the form

$(N-1)T_w \left(1 \mp \frac{2v_r}{c}\right)$ where an additional factor of 2 appears due to the round-trip path to the spacecraft. Thus for these

two scenarios the PPM receiver clock frequency, f_c must be trimmed by $\frac{f_c}{\left(1 \mp \frac{v_r}{c}\right)}$ or $\frac{f_c}{\left(1 \mp \frac{2v_r}{c}\right)}$ (retro-reflected paths) per

pulse arriving interval. Table 1 below shows some typical values for the maximum change in frequency for a 200 MHz clock receiver. Also shown in table 1 are the maximum expected Doppler shifts in the laser wavelength assumed centered at 1064 nm.

Table 1

$f_c = 200$ MHz	Maximum radial velocity (Km/sec)	Max receiver clock Δ (KHz)	Maximum Doppler Shift @ 1064nm (nm)
LEO satellite (400-600 Km altitude)	8	5	.02
Retro-link to LEO satellite (400-600 Km altitude)	8	11	.04
Spacecraft orbiting Mars	21	14	.07
Flyby event	28	19	.09

Table 2 shows the expected photon return expected from retro-reflected links from LAGEOS⁵ and TOPEX/POSEIDON⁶ for transmitting an average of 5 W laser power at pulse repetition rates ranging from 10K -100K pulses per second. These results were estimated assuming a 1-m diameter, receiving telescope. Furthermore the return for a single retro-reflector is estimated, though typically a larger number will contribute to the signal. If a burst of laser pulses with a duration equal to the round trip light time were transmitted from the ground, followed by an equal duration for receiving the pulse sequence prior to sending the next burst, then the number of received pulses with the mean photons per pulse are estimated. Table 2

shows that enough pulses and signal levels are returned in both cases to demonstrate the capability of the PPM receiver to acquire and establish synchronization with a PPM sequence.

Table 2

	Round trip light time zenith angles 12-60° (ms)	Number of pulses in single burst with round trip light time duration	Estimated photon return per pulse per retroreflector
LAGEOS (5900 Km circular orbit)	19-57	197-575 @ PRR = 10K pulses/sec	7-30
TOPEX/POSIEDON (1336 Km circular orbit)	4-13	445-1302 @ PRR = 100K pulses/sec	135-1302

4. SLOT SYNCHRONIZATION

Before slot synchronization is established, the receiver is cognizant of time only in terms of its own clock cycles. While it is assumed that the transmitter and receiver clocks run at approximately the same rate, time-varying propagation delays and small differences between the two clock rates have to be taken into account. The receiver initiates the slot synchronization cycle by starting to count at an arbitrary clock edge, designating that instant as the start of the first subslot. Taking as an example noiseless photon-counting, the receiver measures the subslot accumulator function for each of $2(M+N)$ subsequent subslots, and records the location of the slot containing the greatest count. In general, the recorded counts will not be equal over two slots, but even if that unlikely event should occur, the receiver may arbitrarily assign the first subslot as the one containing the pulse. Note that it is possible (although not very likely) that no counts whatsoever are observed over the entire frame, in which case the acquisition process is repeated until at least one count is observed.

After finding a subslot with a maximal count, the acquisition algorithm defines that subslot as the first half of a valid slot, and forms the first error signal $e_1 = N_{11} - N_{12}$. The synchronization assembly then repeats this process for a predetermined number of frames, K , and forms the sum-error signal

$$E = \sum_k e_k \quad (1)$$

which is the "synchronization statistic" that will be used for adjusting the receiver clock. If most of the laser pulse falls within the first subslot the average error signal tends to be positive, otherwise it is negative (with high probability). If positive, the clock is advanced by a small amount, if negative it is delayed. Obtaining a value close to zero for the error signal implies that the slots are essentially synchronized with the received laser pulses by chance, hence no additional delays need to be applied.

Note that whereas the subslot observables are Poisson distributed random variables, their difference is not. The mean of the difference is the difference of the means, and the variance is the sum of the variances:

$$e_i = \bar{N}_{i1} - \bar{N}_{i2} \quad (2a)$$

$$\text{var}(e_i) = \bar{N}_{i1} + \bar{N}_{i2} \quad (2b)$$

where \bar{N}_{ij} , $j = 1, 2$, refers to the average count in the j -th subslot of the i -th slot. The density for the sum of K slot differences can be obtained directly by noting that the resulting random variable is equivalent to the sum over the second subslot subtracted from the sum over the first subslot over K slots. Letting S_1 be the sum over the first subslot for K slots and S_2 the sum over the second subslot for K slots, the difference statistics can be expressed as

$$E = \frac{1}{K} \sum_{i=1}^K e_i = \frac{1}{K} \sum_{i=1}^K (N_{i1} - N_{i2}) = \frac{1}{K} \sum_{i=1}^K N_{i1} - \frac{1}{K} \sum_{i=1}^K N_{i2} \equiv S_1 - S_2 \quad (3)$$

Because the partial sums are themselves Poisson processes, their mean and variance is given by

$$\bar{S}_j = \frac{1}{K} \sum_{i=1}^K \bar{N}_{i,j}, \quad j=1, 2 \quad (4a); \quad \text{var}(S_j) = \frac{1}{K^2} \sum_{i=1}^K \bar{N}_{i,j}, \quad j=1, 2 \quad (4b)$$

This leads to the mean and variance of the "K-sum" differences as

$$\bar{E} = \bar{S}_1 - \bar{S}_2 \quad (5a); \quad \text{var}(E) = \text{var}(S_1) + \text{var}(S_2) \quad (5b)$$

The probability density for the difference of two Poisson random variables has been derived by Pratt in [11]. Substituting the variables defined above yields the density

$$P(E = j | \text{signal slot}) = \left(\frac{\bar{S}_1}{\bar{S}_2} \right)^{-j/2} \exp[-(\bar{S}_1 + \bar{S}_2)] I_{|j|} \left[2\sqrt{\bar{S}_1 \bar{S}_2} \right] \quad (6)$$

This density, together with the second-order statistics defined in ref. 7 completely characterizes the error signal used to update the PPM slot-synchronization system with photon-counting detection, provided the "signal-slot" has been identified correctly. However, the signal-slot is identified correctly most of the time under normal operating conditions, since deep-space communications links are typically designed to operate with uncoded symbol-error probabilities of approximately 10^{-2} . The only effect of an occasional detection error is to reduce the expected value and variance of the partial sums, since noise-slots have less optical energy than signal-plus-noise slots.

The analysis for the case of APD detection parallels the derivation for the photon-counting case, except that Poisson random variables are now replaced by Gaussian random variables. Again assuming that the synchronization assembly uses only signal slots to obtain the error signal (almost always true under nominal operating conditions), the mean of the error signal is the difference of the means and the variance the sum of the variances of the subplot observables.

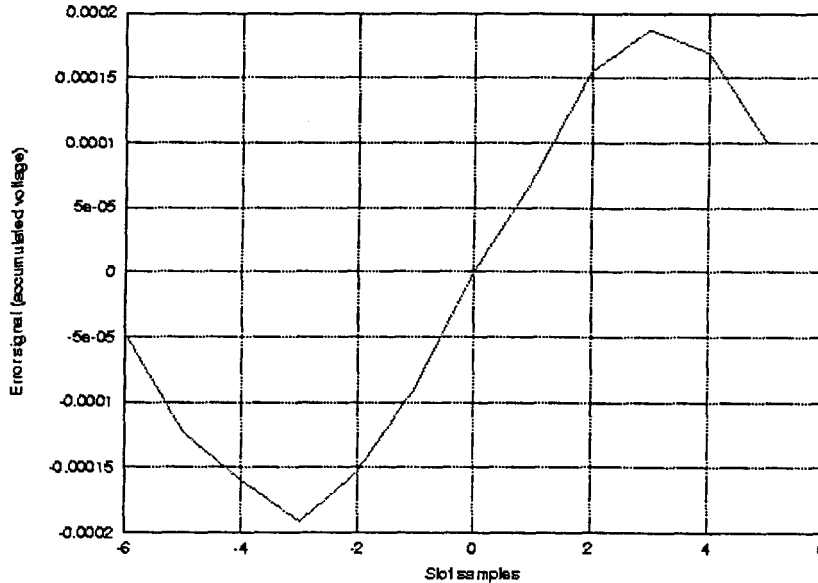


Figure 5. Measured "S-curve" obtained with an APD detector measuring a PPM sequence of 532 nm laser pulses

The average value of the error signal depends on the time-delay Δ between the slot-boundaries defined by the receiver, and the relative delay of the received pulses over a K-frame averaging interval. If the receiver is well synchronized, then the error signal should be zero, otherwise a positive or negative error signal is developed that is used by the synchronization assembly to re-center the pulses within the slots defined by the receiver. The magnitude of the error signal typically increases as the pulse drifts away from zero, but reaches a limit and actually starts decreasing as the pulse begins to drift outside the slot. The function defined by the average error signal plotted in terms of the delay offset is called an "S-curve" in the synchronization literature. An example of a measured S-curve obtained with an APD detector⁸ responding to PPM pulses from a doubled

Nd:YAG laser is shown in Fig. 5. Closed-loop performance of the linearized synchronization assembly depends on the slope of the S-curve at zero, and on the total loop gain and any additional filtering before applying the K -sum error signal to the receiver clock.

5. ANALOG SIGNAL CHAIN (ASC)

The PPM-ASC design architecture is derived from consideration of: (1) detector response (2) laser pulse shape/width (3) frame rate (4) analog-to-digital (ADC) domain, resolution, sample rate and aperture (5) link dynamics.

The detector response determines overall ASC bandwidth and gain requirements. The laser pulse frequency spectrum convolved with the detector response defines an "optimal" filter response for the ASC to minimize noise bandwidth. The PPM frame rate establishes the lower bounds of ASC bandwidth. The ADC parameters establish the upper bounds of the ASC bandwidth and affects gain considerations. The ADC sample aperture is assumed to be small enough to not significantly reduce the digitization bandwidth from the Nyquist limit. The sample aperture error is folded into the effective resolution parameter. Link dynamic features such as fluctuations in received laser pulse heights must be taken into account. The source of the signal fluctuation may be the inherent intensity variations in q-switch laser output, additional fluctuations due to pointing jitter at the laser transmitter and finally atmospheric turbulence induced fluctuations (for large aperture receivers these tend to average out).

Figure 7 depicts the generic PPM-ASC topology. The post-amp block maps the detector voltage output (range) to the ADC input (domain) with the goal of minimal noise addition. The optimal filter block matches the ASC transfer response to the expected pulse response to minimize the processed noise bandwidth. The minimal implementation of the optimal filter block would be a bandpass filter, with a low frequency limit set by the frame rate and the high frequency limit set by Nyquist sampling considerations. The clamp amplifier block protects the ADC from signal excursions outside of its nominal conversion domain.

The APD ASC design is driven by the large post-amp gain required to match the expected small signal amplitude to the ADC domain. Three design topologies are considered for the APD post-amp, namely, (1) fixed gain (2) linear gain controlled and (3) logarithmic approximation. The fixed gain solution is depicted in Figure 7. A multi-stage amplifier chain is required due to gain-bandwidth (GBW) product limitations of available low-noise amplifier gain stages.

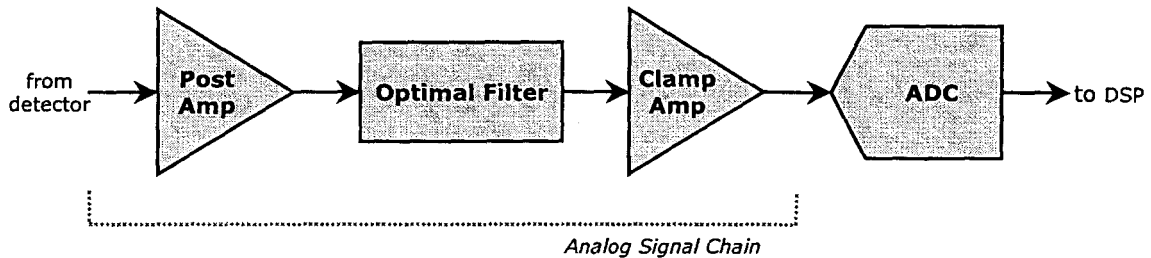


Figure 6: Generic PPM analog signal chain architecture.

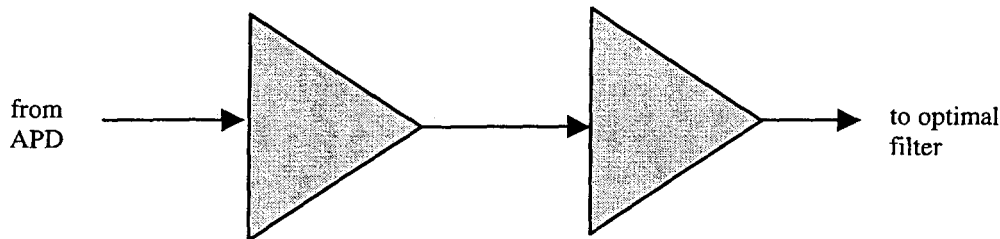


Figure 7. Fixed gain APD post-amplifier topology.

The primary advantage to a fixed gain solution is that COTS low-noise, fixed-gain amplifiers are readily available. A linear multiplier stage may be added after the first amplifier stage to accommodate larger link power fluctuations. This topology is depicted in Figure 8.

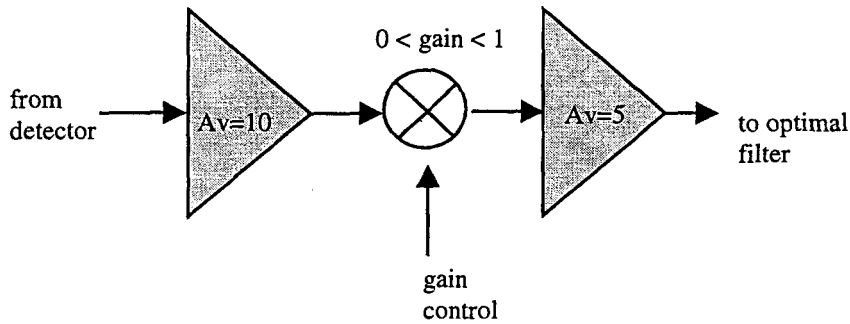


Figure 8 Variable gain APD post-amplifier topology.

The gain control signal comes either from a manual control or from the bandlimited output of an AGC loop. The variable gain topology is a simple solution to accommodate a larger input signal dynamic range, although at the expense of some additional noise. A COTS implementation of this solution has not yet been identified. The third post-amp topology considered eliminates the need for a gain control loop by approximating a logarithmic response by summing the output from a series of domain-limited amplifiers. This topology is depicted in Figure 9.

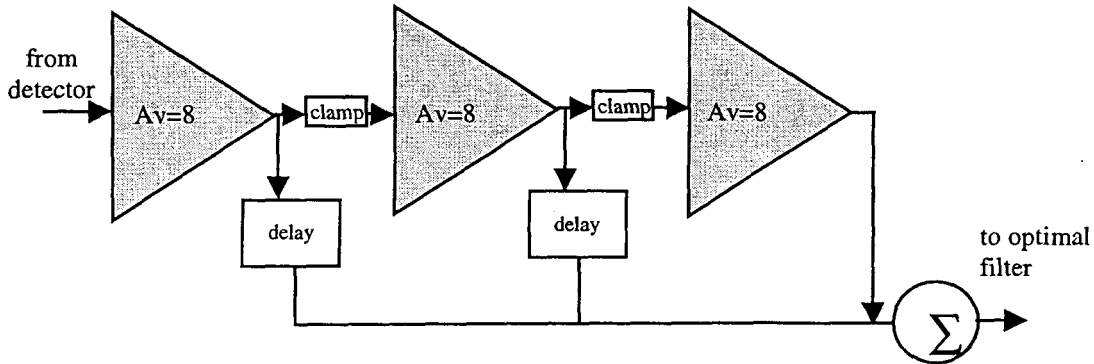


Figure 9 Logarithmic approximation APD post-amplifier topology

Figure 10 compares the transfer function of this topology with a true logarithm response.

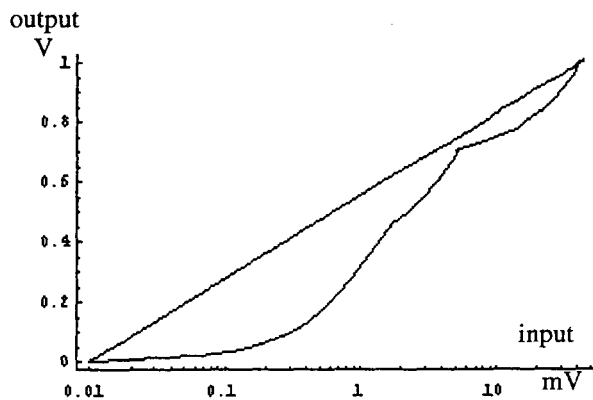


Figure 10 Transfer function for the proposed logarithmic amplifier compared to an ideal logarithmic response (straight line)

Although the logarithmic approximation post-amp is the most complicated ASC design considered here, and requires a custom implementation, it has the potential to maximize the efficiency of data acquisition during field tests by minimizing the effects of link dynamics.

Ignoring dark current (for now) and requiring that at least one photon be detected per frame, an initial estimate of the mean detector signal amplitude for a given frame error rate can be made as,

$$\bar{N}_{pulse} = \frac{Q_e \log FER}{\log(1 - Q_e)} \quad (7)$$

where, \bar{N}_{pulse} is the mean number of detected photons per pulse; FER is the allowable frame "non-detect" rate; and Q_e is the nominal detector quantum efficiency at the signal wavelength which further reduces to $\bar{N}_{pulse} = \log FER$ for low Q_e .

A second factor to consider is the PMT anode current limit, as this relates to the maximum frame rate and link dynamics (maximum signal level). Starting with an upper bound on the frame rate at the nominal signal level,

$$PRF_{max} = \frac{I_{anode\ limit}}{\bar{N}_{pulse} G} \quad (8)$$

where, PRF_{max} is the frame rate upper bound; $I_{anode\ limit}$ is the PMT anode current limit; and G is the PMT gain. The available link "headroom" in db can then be defined as,

$$10 \log_{10} \frac{PRF_{max}}{PRF_{nom}} \quad (9)$$

where PRF_{nom} is the nominal frame rate.

The optimal filter module should ideally pass only those frequency/phase components that fit the detector response to the signal laser pulse. This minimizes the system bandwidth, and therefore also minimizes the noise bandwidth to maximize the detector signal/noise ratio. However, using typical q-switched laser pulses, as well as, actual laser pulse shapes recorded with detectors in the laboratory the optimal filter provided only 0.1 dB of improvement in signal-to-noise over a simple bandpass filter. Therefore a simple bandpass filter with extending from 100 KHz to 100 MHz shall be sufficient for this application

The final clamp amplifier to limit the ADC domain is simply required to have a 100 MHz bandwidth and unity gain. It should have a moderately low equivalent input noise, and ideally will also be able to directly drive the selected ADC input impedance requirement.

6. DIGITAL SIGNAL PROCESSING ASSEMBLY

For this initial receiver design a nominal digital sampling rate of 200 MS/s will be assumed, giving a minimum subslot width of 5 ns. Since there are always at least two subslots per slot, the minimum slot width is 10 ns. As described in section 4 subslots are used to center the pulse in a slot (subslots are summed separately and passed to the CPU for synchronization decisions). The slot width will be user specified in units of 10 ns. Dead time will be specified in units of slots. There will generally be 256 slots per frame, which could be changed to include 64 or 128 later. Frame synchronization shall be achieved by pre-calibration of known (constant) data.

Processing consists of identifying the slot number of the largest pulse (sum of subslot values) as described in section 4. The amplitude of this pulse is stored. The raw slot amplitudes will be supplied on a connector along with a slot and frame strobe, and a limited number of these samples will be captured and written to disk. The derived bytes and their amplitude will be supplied on a connector along with a strobe. The same information is recorded on disk. A block diagram diagram of the digital assembly with external interfaces is shown in Figure 11.

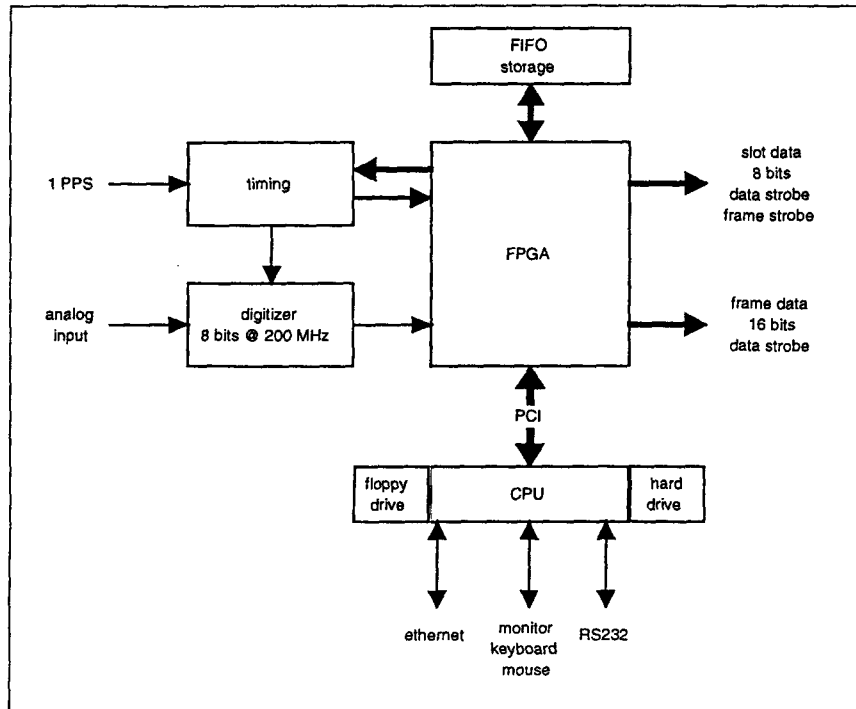


Figure 11 Block diagram of the digital signal processing assembly (DSPA).

The 200 MHz clock will be derived from a crystal VCO whose frequency can be varied by about +/- 50 ppm to account for the relative motion of the transmitter and receiver that would normally occur. The CPU will alter the frequency of the VCO in order to achieve and maintain slot synchronization based on sub slot sums provided by the FPGA. The digitizer is an 8-bit analog to digital converter (ADC) running at the VCO rate of (nominally) 200 MHz. The FPGA does most of the work. It is a Xilinx Virtex II one million gate programmable device and hence the receiver is highly reconfigurable which allows considerable flexibility in signal processing. The CPU is a standard PC which communicates with the FPGA via the PCI bus and possibly interrupts and will be involved in user interface, configuration, frame synchronization, slot synchronization and data recording.

7. CONCLUSIONS

In this report analysis and discussions along with the design of a PPM receiver have been presented. The PPM receiver is being assembled at JPL during the next year and will be utilized for a series laboratory followed by field tests. The emphasis of the testing will be to enable a thorough evaluation of all issues that relate to deep space optical communications from interplanetary distances. The single major technology validation that will be accomplished as a result of building and testing the PPM receiver will be the efficiency of algorithms for symbol detection and synchronization that are currently baselined but have not been rigorously tested. In addition the PPM receiver will enable gathering of larger slot statistics for a variety of detectors, a capability that is currently rather limited using state of the art stand alone digitizers and storage oscilloscopes. The PPM receiver will also provide capability for testing additional functions such as decoding and ranging that will be functional features of an operational PPM receiver. With the experience gained through some of the planned development and testing described in this report, and taking advantage of technology maturity in faster digitizers and perhaps more sensitive detectors expected in the next 2-3 years, we will be ready to develop and deliver an advanced PPM receiver by the 2004-2005 time frame.

ACKNOWLEDGEMENTS

The authors are grateful to Meera Srinivasan for providing analyzed data on slot synchronization. Helpful discussions with J. Hamkins, N. Lay, J. Lesh and H. Hemmati are also gratefully acknowledged. The research described was carried out with funding from the Inter-Planetary Network and Information Systems Technology (IPN-IST) Program Office, Jet Propulsion Laboratory, California Institute of Technology, under contract with the National Aeronautics and Space Administration. *at the*

REFERENCES

1. C.-C. Chen, J. W. Alexander, H. Hemmati, S. Monacos, T. Yan, S. Lee, J. R. Lesh and S. Zingales, "System Requirements for a Deep Space Optical Transceiver, "Proceedings of SPIE, Free-Space Laser Communications Technologies XI, [Ed. G. S. Mecherle], 3615, 1999
2. C.-C. Chen, "Figure of Merit for Direct-Detection Optical Channels, " TDA Progress Report 42-109, 136
3. G. G. Ortiz, J. V. Sandusky and A. Biswas, " Design of an opto-electronic receiver for deep-space optical communications, " JPL Telecommunications Mission Operation Progress Report, 42-142, August 2000.
4. A. Biswas, B. Madden-Woods, M. Sriivasan, V. Vilmrotter, W. Farr, "Ground detectors for optical communications from deep space, "Proceedings of SPIE, Free-Space Laser Communications Technologies XI, [Ed. G. S. Mecherle], 4272, 2002 (In Press).
5. J. J. Degnan, "Satellite Laser Ranging: Current Status and Future Prospects, " IEEE Trans. Geoscience and Remote Sensing, GE-23398, 1985.
6. J. A. Schwartz, "Laser ranging error budget for the TOPEX/POSEIDON satellite, " Appl. Opt., 29, 3590, 1990.
7. W. K. Pratt, *Laser Communications Systems*, John Wiley & Sons, New York, 1969.
8. M. Srinivasan, J. Hamkins, B. Madden-Woods, A. Biswas, and J. Beebe, "Laboratory Characterization of Silicon Avalanche Photodiodes (APDs) for Pulse-Position Modulation (PPM) Detection", IPN Progress Report 42-146, August 15, 2001.